Journal of Molecular Structure 1206 (2020) 127739

Contents lists available at ScienceDirect

Journal of Molecular Structure

journal homepage: http://www.elsevier.com/locate/molstruc

Substantial effect of silk fibroin reinforcement on properties of hydroxyapatite/silk fibroin nanocomposite for bone tissue engineering application

J. Mobika , M. Rajkumar *, V. Nithya Priya , S.P. Linto Sibi

Department of Physics, PSG College of Arts and Science, Coimbatore, Tamilnadu, India

ARTICLE INFO

Article history:
Received 31 October 2019
Received in revised form
3 January 2020
Accepted 14 January 2020
Available online 15 January 2020

Keywords:
Biodegradability
Hydroxyapatite
Silk fibroin
Biomineralization
In-situ co-precipitation method

ABSTRACT

Nano-biocomposites that mimics bone's extracellular matrix with hydroxyapatite as an inorganic and silk fibroin as organic phase for three different ratios via a simple *in-situ* co-precipitation method have been synthesized. The silk fibroin, a biodegradable polymer from cocoons of *Bombyx mori* silkworm were extracted by employing a chemical-free High-Temperature High-Pressure method as a degumming route. Then followed by the regeneration process which was done by using calcium chloride-formic acid solvent system to replace time-consuming, cost-effective traditional methods. The prepared composites were structurally analyzed using Fourier Transform Infra-Red spectroscopy (FTIR) and X-ray Diffraction (XRD) techniques. The morphology and the elemental composition of the nano-biocomposites were examined using Field Emission Scanning Electron Microscopy (FESEM) and Energy-dispersive X-ray Spectroscopy (EDX). The *in-vitro* bioactivity of the bio-composites namely, swelling ratio, biodegradation and biomineralization ability is monitored in the presence of Simulated Body Fluid (SBF). Our observation demonstrate that silk fibroin concentration influences the formation of hydroxyapatite.

1. Introduction

Over a few decades, major portion of the humankind suffers from bone defects which is mainly due to aging, tumor, trauma and other factors like estrogen deficiency [1,2]. One of the most challenging problem is to empathize the suitable method and material to mend the bone defects caused to the elderly patients by skeletal diseases, tumors and traumatic injury. The deficiency of ideal bone tissue leads to an increase in health issues. Therefore, bone substitutes or bone defect therapy proves to be a better solution to solve the problem. Conventional therapies for bone defects or bone substitution consist of autografts and allografts that provide a fast osteointegration with the surrounding tissues after implantation [3–6]. However, conventional bone therapy has encountered some limitations such as the threat of infection, immune response and donor shortage, as well as donor site morbidity. Therefore, an alternative method is imperative to repair bone defects. Artificial bone graft is one of the most emerging alternate to repair and reproduce bone defects, which would be a great advantage in the field of biomedical engineering. Researches on bone tissue engineering over the past decades have inspired innovation in the field of artificial scaffold [7]. An artificial scaffold for bone defect must be biocompatible, biodegradable and should facilitate mechanical support during repair and regeneration of damaged or diseased bone tissue. Researchers have focused on the development of the scaffolds to promote and regenerate the tissues with required porosity. Artificial scaffold with good porosity efficiently aids the osteoblast cell proliferation and osteogenesis within a short period of time [8]. Recently, bioactive calcium phosphate-based scaffolds are used as bone fillers and bone substitutes [9]. Among various compositions of calcium phosphate, hydroxyapatite has exquisite biocompatibility and it is a natural component of bone with similar chemical ratio [10,11]. In addition, it acts as an excellent temporary substrate that allows cell in-growth, proliferation and differentiation [12,13]. In recent years, great attention has to be made to manipulate the properties of hydroxyapatite (HAP) to enhance stiffness, biodegradability, osteoconductivity, osteoinductivity, etc., by modifying the HAP structure employing doping or dispersing the HAP on polymer or carbon materials [14–16].

Numerous polymeric matrices have been utilized for this concern including the synthetic biodegradable polymers such as

* Corresponding author.
E-mail address: vmanirajkumar@gmail.com (M. Rajkumar).

https://doi.org/10.1016/j.molstruc.2020.127739
0022-2860/

poly (lactic acid) (PLA), poly (ε-caprolactone) (PCL), poly (glycolic acid) (PGA) and natural polymers such as chitosan, hyaluronic acid, alginate, dextran, collagen, gelatin, elastin and silk fibroin [17–19]. In comparison with other biopolymers, Silk fibroin (SF) has provoked progressive attention in bone tissue engineering application because of its controllable degradability, abundant hydrophilic polar groups, biocompatibility, non-toxicity and mechanical properties [20,21]. Moreover, SF is a natural polymer and it enhances the osteoconductivity without causing any adverse effect to the surrounding tissues. Due to the presence of degradable material in SF, it deteriorates itself without any toxic effects and it provides nutrients for tissues. Interfacial chemical bonding between HAP and SF provides exceptional properties to repair the defects. SF proteins play a vital role in the mineralization of HAP [22]. Thus, it has been extensively used in biomedical applications such as bone tissue engineering, skin tissue engineering, drug delivery, wound dressing and so on.

Most of the composites are fabricated from the simple mixing of inorganic and organic phases resulting in nanocomposites with very limited interaction between these two phases [23–27]. To overcome this problem, we adopted the *in-situ* biomimetic co-precipitation method to synthesis HAP/SF nanocomposites. During the formation of the HAP/SF composite, SF act as an organic matrix to provide active sites for the nucleation and growth of HAP crystals. The ratio of HAP and silk fibroin nanocomposite is optimized to achieve better bioactivity of the composite. Optical, structural, morphological and *in-vitro* bioactivity details of these composites examined in simulated body fluid (SBF) are discussed below.

2. Materials and methods

2.1. Degumming of silk fibroin

The degumming process was opted to extract silk fibroin from cocoons of *Bombyx mori* (*B.mori*) by high temperature and high pressure (HTHP) method [28]. In concise, raw cocoons were chopped into pieces and autoclaved at 120 °C for 30min with a material-to-liquid ratio (cocoons: deionized water) of 1:50. The degummed material was then rinsed thoroughly with warm water and squeezed out to remove sericin. The extracted silk fibroin were dried at 40 °C. The degumming ratio of the prepared silk fibroin was found to be 27%.

2.2. Regeneration of silk fibroin

In order to acquire regenerated silk fibroin, an aqueous solution of formic acid-$CaCl_2$ was employed to enhance the mineralization and degradation properties of silk fibroin [29]. The aforementioned degummed silk fibroin (SF) was dissolved in the aqueous solution for about 1 h to get a 6 wt% solution. Then, the SF- $CaCl_2$-formic acid solution was poured into a polystyrene Petri dish to form an SF film. The system was facilitated with good air circulation for quick evaporation of formic acid within 24 h. The resultant product was treated with water for 6 h and dried at room temperature to obtain the regenerated silk fibroin film.

2.3. Preparation of hydroxyapatite/silk fibroin nanocomposite

HAP/SF nanocomposite was prepared via an *in-situ* co-precipitation route from the Calcium (Ca) and Phosphorus (P) precursors with the stoichiometric ratio of Ca/P = 1.67 [30]. Initially, an aqueous solution of silk fibroin (6 wt %) was prepared by dissolving SF film in formic acid and cross-linked with glutaraldehyde (1 v/v %) for 30 min under vigorous stirring. A stoichiometric amount of Ca and P precursor solution were added one-by-one dropwise into the SF solution at 60 °C. The pH of the solution was adjusted to about 10 by a weak base (liquid ammonia). Overnight stirring was employed and then obtained slurry was left aging for 24 h at room temperature. Finally, the aged samples were centrifuged at 3000 rpm and washed several times with water to recover the HAP/SF composites without any impurities. The obtained silk fibroin/hydroxyapatite composite was synthesized at three different ratios of 2:3 (HS-1), 1:1 (HS-2) and 3:2 (HS-3). Pristine HAP was fabricated by the same procedure without the addition of silk fibroin.

2.4. Biomineralization of HAP/SF nanocomposites

The formation of biominerals on the surface of a prepared specimen was evaluated in the SBF solution. This blood plasma like solution was prepared as described in the literature [31] by dissolution of the following chemicals in the order: NaCl, $NaHCO_3$, KCl, $K_2HPO_4 \cdot 3H_2O$, $MgCl_2 \cdot 6H_2O$, $CaCl_2$ and Na_2SO_4 in distilled water, and then buffered to pH 7.40 with tris hydroxymethyl aminomethane (Tris) and HCl solution at 37 °C. Equi amounts of the samples were taken to prepare the pellet with uniform size. The prepared pellets were immersed separately into a plastic bottle with an equal volume of SBF solution at 37 °C for 15 days during which the SBF solution was left undisturbed. After 15 days of immersion, the samples were taken out and washed with distilled water to clear out the adsorbed material. Finally, the specimens were dried and characterized using FTIR and XRD to affirm the biomineralization ability.

2.5. Swelling and biodegradation test

The swelling and biodegradation behavior of the scaffold was investigated by immersing equal shaped disc into the SBF solution maintained at human body temperature for a different period of time (1, 6, 11 and 15 days). At the end of each specified time period, wet weight was calculated after blotting the scaffold with a filter paper. The swelling ratio is measured from the following equation [32].

$$SR(\%) = [(w_w - w_0)/w_0] \times 100 \quad (1)$$

where, w_o and w_w are the original and wet weight of the scaffold respectively.

Biodegradation was measured by calculating the dry weight after the different incubation periods, which is obtained from the following equation [33].

$$WL(\%) = [(w_0 - w_d)/w_0] \times 100 \quad (2)$$

where, w_o and w_d are the original and dry weight of the scaffolds respectively.

3. Result and discussion

3.1. Structural and morphological analysis

3.1.1. Influence of SF incorporation on the vibrational bands of hydroxyapatite

FTIR spectroscopy has been carried out to analyze the inter and intra-molecular bonding between HAP, SF and their composites. FTIR spectra of the prepared samples are shown in Fig. 1 and the inset of Fig. 1 depict the vibrational spectrum of Silk fibroin. The corresponding absorption bands are summarized in Table 1. The bands of amide-I (C═O stretching) and amide-III (C–N stretching

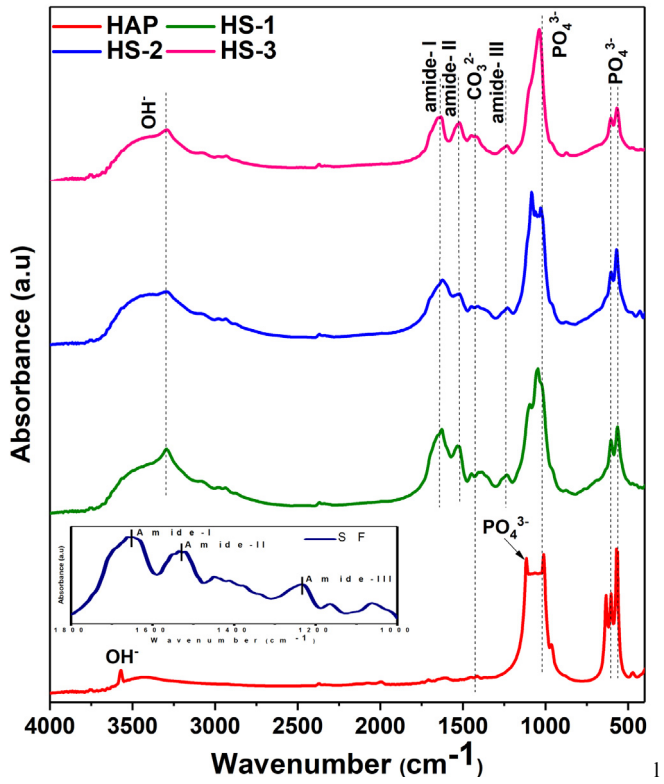

Fig. 1. FTIR spectra of Pristine HAP, SF, HS-1, HS-2 and HS-3 nanocomposites.

and C═O bending) were found at 1651 cm^{-1} and 1234 cm^{-1} respectively which is due to a random coil conformation [34]. The band present at 1519 cm^{-1} belongs to stretching and bending modes of amide II (C–H and N–H) group and it confirms the formation of the β-sheet structure [35]. It could be concluded that the β-sheet and random coil structures coexist in the samples.

The characteristic bands of HAP show four modes of vibration for PO_4^{3-}. A strong characteristic band at 470 cm^{-1} attributed to symmetric bending mode of O–P–O and the band appearing at 1010-1120 cm^{-1} are assigned to asymmetric stretching of P–O in PO_4^{3-} [36]. A shoulder band at 964 cm^{-1} represents the symmetric stretching mode of P–O and bands at 567 cm^{-1} and 602 cm^{-1} corresponds to the asymmetric bending mode of O–P–O in PO_4^{3-} [37,38]. The OH^- stretching and bending vibration bands are present at 3572 cm^{-1} and 632 cm^{-1}, respectively [39]. A very small band at 1421 cm^{-1} can be seen which is due to the presence of few CO_3^{2-} groups and it suggests that the presence of B-type carbonate apatite along with pure apatite originated from the absorption of CO_2 from the atmosphere [40]. Young bones contain B-type carbonated apatite which could help the bone maturation [41]. The band at 3425 cm^{-1} and 1604 cm^{-1} are due to O–H stretching and H–O–H bending modes of vibration which indicates the presence of water molecules in the HAP.

Comparing the spectra of composite materials (HS-1, HS-2 & HS-3) with pristine HAP and SF, it could be observed that band associated with HAP and SF are present with a slight shift in band values signifying that HAP was incorporated into SF. The band position of amide-I in HS-1, HS-2, and HS-3 shifted from 1651 cm^{-1} to 1621, 1624 and 1627 cm^{-1} which indicates that some random coil converted into the β-sheet structure. It is well known that SF molecules can rearrange to form a crystalline structure due to the change in hydrogen bonding caused by cross-linking agent glutaraldehyde. The PO_4^{3-} absorbance band (1010-1120 cm^{-1}) is widened and the intensity of amide bands is decreased in composites. The composites are less carbonated compared to that of pure HAP which indicates less potential for the carbonation of the HAP phase due to the highly active interaction between HAP and the polymer matrix during the process stage. SF contains many carboxyl groups which provide the nucleation sites for HAP molecules. Initially, Ca^{2+} ions bind to the active surface (-COOH) of SF and form -$COOCa^+$ ions. Afterward, phosphate ions are attached to these groups. Alkaline solution promotes this action and facilitates apatite deposition and growth [42].

3.1.2. *Influence of SF incorporation on the phase and crystallite size of the hydroxyapatite*

Crystallographic characteristics of pristine HAP, SF and HS composites were studied by XRD analysis and the results are shown in Fig (2(a–d)). The inset of Fig. 2 confirms the presence of silk-II (β-sheet) and silk-I (random coil) structure of SF at $2\theta = 20.6°$ and 24.2°, respectively [43,44]. The typical diffraction peaks of hexagonal-HAP have been noticed at 26.0°, 28.2°, 29.0°, 31.9°, 32.3°, 34.1°, 39.9° and 46.9° which are in good agreement with the standard database (ICDD card no. 09–0432). They also reveal the unique crystalline phase of HAP and the absence of no processing residues or secondary phase (TCP) in the sample [45,46]. The sharp and high intense peaks with a slight shift in the peak position without change in the HA phase were obtained after incorporation of SF. The characteristic planes (211) and (300) of HAP were sharp and distinct in pristine HAP. In the case of composites, these two peaks were companied into a broad peak which implies the poor crystalline nature of the prepared composites due to the size effect

Table-1
FTIR vibrational bands of pristine HAP, SF and their composites.

Wavenumbers (cm^{-1})					Vibrational assignment	Reference
HAP	SF	HS-1	HS-2	HS-3		
470	–	474	478	478	β_{sym}O-P-O	[36]
567,602	–	563,601	570,601	567,605	β_{asym}O-P-O	[38]
632	–	–	–	–	γO-H	[39]
964	–	963	962	965	ν_{sym}P-O	[37]
1010–1120	–	1010–1120	1010–1120	1010–1120	ν_{asym}P-O	[36]
_	1234	1234	1230	1234	Amide-III	[34]
1421	–	1436	1436	1436	νCO_3^{2-}	[40]
_	1519	1516	1519	1519	Amide-II	[35]
1604	–	–	–	–	β_{sym}H-O-H	
_	1651	1621	1624	1627	Amide-I	[34]
3425,3572	–	3394	3375	3390	νO-H	[39]

ν – stretching, β – in-plane bending, γ – out-of-plane deformation, sym – symmetric, asym – asymmetric.

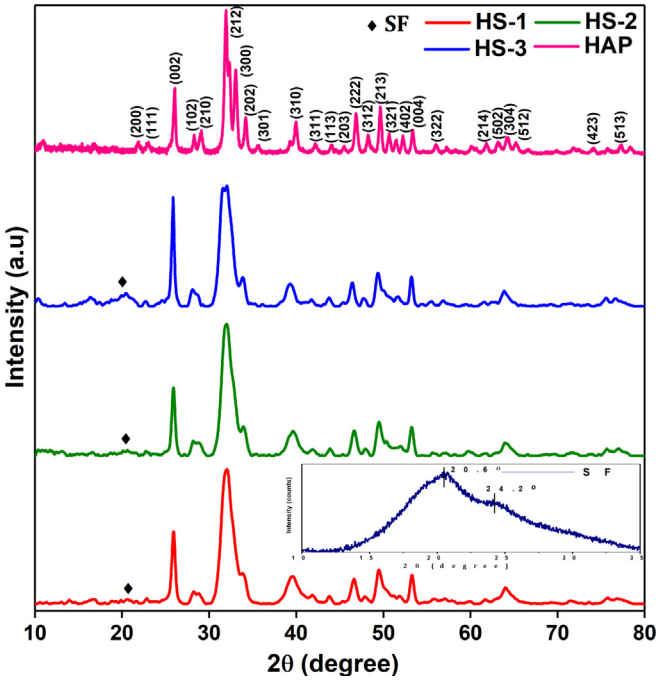

Fig. 2. XRD pattern of Pristine HAP, SF, HS-1, HS-2 and HS-3 nanocomposites.

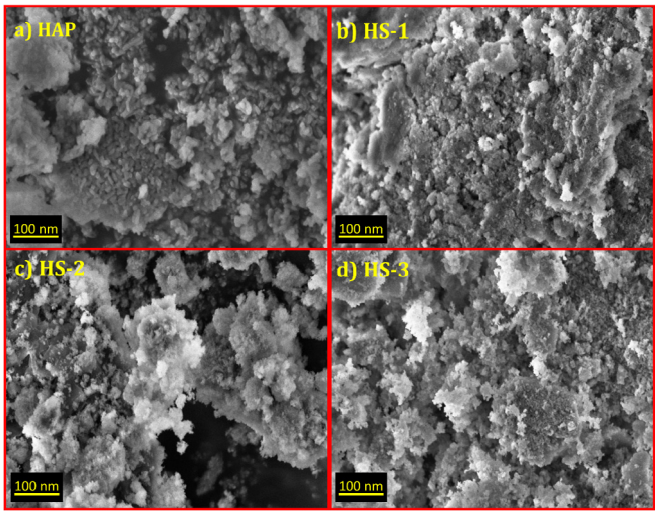

Fig. 3. Morphology of (a) pristine HAP (b) HS-1 (c) HS-2 and (d) HS-3 nanocomposites.

of HAP during *in-situ* crystal formation on the polymer matrix. Composites exhibit a broad halo peak at 20.1° arose from the conversion of some random coil structure into the β-sheet structure during the chemical cross-linking process. This peak was very weak in the diffraction pattern of HS-3 and almost vanishes in HS-1 likely due to the decrease in SF content. The difference in the peak intensity with SF ratio confirms the successful addition of HAP in SF matrix. A decrease in the peak intensity and broadening of peaks leads to an increase in the surface area of the composite. From the literature, the low crystalline nature of the composites preferentially enhances the new bone formation [47]. Crystallite size (D) of the samples were calculated using the Scherrer formula [48].

$$D = [k\lambda/\beta\cos\theta] \quad (3)$$

The calculated average crystallite size of the pristine HAP, HS-1, HS-2, and HS-3 were 30, 22, 17 and 14 nm, respectively. The crystallite size of the nanocomposites decreases with increase in the SF ratio. The decrease in the crystallite size of the composite enhances cell proliferation, integration and degradation.

3.1.3. *Influence of SF incorporation on the morphology of hydroxyapatite*

The surface morphology of the prepared nanocomposites with different weight ratios of three dissimilar composites and pristine HAP were analyzed using FESEM and shown in Fig. 3. Pristine HAP particles are in needle-like structure with a length of 90–120 nm and width of 10–20 nm. The majority of the rod-like nanoparticles were of regular shape with some agglomeration [49]. The morphology of HAP nanoparticles is significantly affected by the addition of silk fibroin. In all composites, HAP particles are aggregated and heterogeneously distributed in SF fibrils but there were no obvious boundaries between the organic phase and inorganic phase. Also, SF played a vital role in controlling the HAP size compared to pristine HAP. This shows the higher affinity of inorganic particles towards organic matrix which is only achieved by the *in-situ* precipitation method. HS-2 and HS-3 composites have some interconnected pores which are beneficial for the circulation of the physiological fluid and tissue in-growth [50]. Due to the presence of higher concentration of HAP, the surface of HS-1 composite consisted of densely packed particles without pores. In composite formation, polar and charged side chains present in silk fibroin acts as the nucleation site. Initially, positively charged calcium ions bind with the SF molecules and the phosphate groups are attracted towards calcium ions through electrostatic interaction. Finally, HAP is formed on the surface of the polymer matrix. This close bonding between the inorganic and organic phases may help to improve the biomineralization ability of the composite.

The EDX spectrum for the HAP nanoparticles and HS nanocomposites are shown in Fig. 4. The spectrum clearly depicts the presence of main constituents of hydroxyapatite such as Ca, P and O in the structure of HAP nanoparticles along with C. The existence of C may come from the environmental CO_2. The difference in the atomic ratio of Ca/P (1.64) is mainly due to the presence of carbonated HAP [51]. Meanwhile, the EDX spectra of the nanocomposites confirm the presence of Ca, O, P and C which indicates that the composite is composed of HA and SF.

3.2. *In-vitro biological analysis*

3.2.1. *Influence of SF incorporation on the biodegradation of hydroxyapatite*

The effect of soaking time and concentration of polymers influences the degradation rate of the scaffolds as shown in Fig. 5. After the specified time period (1, 6, 11 and 15 days), all scaffolds exhibit some amount of weight loss. Overall weight loss of all scaffolds was less than 12% after 15 days. The degradation rate of pristine HAP was witnessed to be slow on comparing with the composites [52]. After incorporation of SF, the weight loss of the composite was increased with increase in the SF ratio that may due to the presence of degradable hydrophilic block in the polymer. Initially, the degradation rate of the HS-3 was higher than 11%, it decreased with increase in the soaking time period. After 15 days, degradation rate was approximately 0.5%, 5%, 7% and 8% for pristine HAP, HS-1, HS-2 and HS-3 scaffolds, respectively. Due to the mineralization process, all the scaffolds exhibited a decreased weight loss with an increase in the soaking time period in the SBF solution. Hu Y et al., reported that the difference in the weight of biodegradable polymer-HAP based scaffolds were attributed to the two competing processes of scaffold degradation and

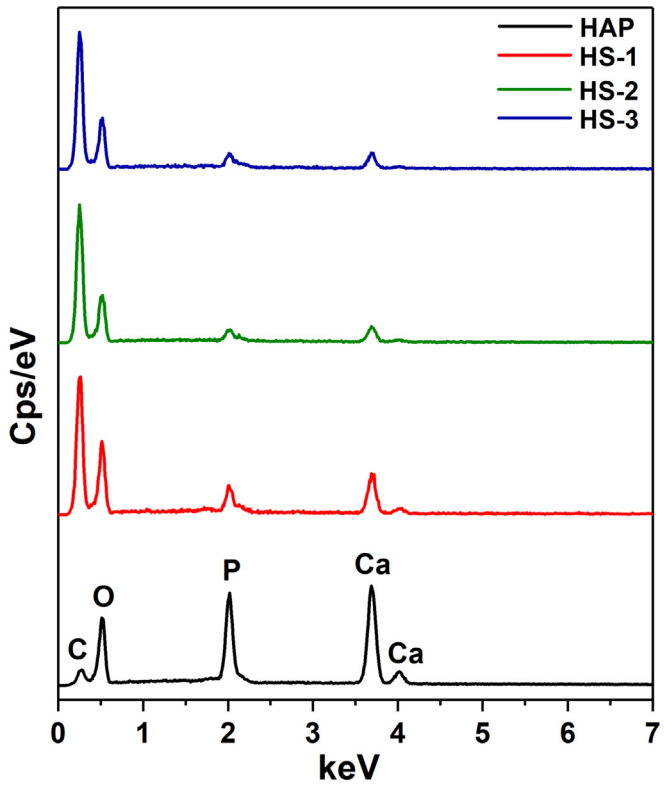

Fig. 4. EDX spectra of pristine HAP and HS nanocomposites.

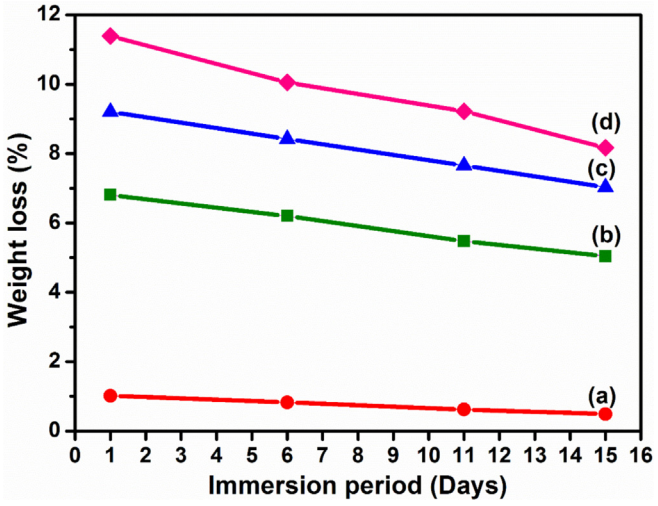

Fig. 5. Degradation rate of (a) pristine HAP (b) HS-1 (c) HS-2 and (d) HS-3 nanocomposites post immersion in SBF solution.

mineralization of apatite [53]. Hence, the decrease in the degradation rate of scaffolds confirms the deposition rates of apatite were greatly increased, which indicates the bioactivity of the prepared composites. The difference in the degradation of the scaffolds is mainly due to the presence of water-soluble random coil structure (silk-I) in it [54]. In the HS-3 scaffold, the amount of SF is higher than the HAP, so it significantly enhances the degradation rate of the HS-3 scaffold compared with other scaffolds. The degraded products of SF were amino acids that can be absorbed either by *in-vitro* or *in-vivo* which is favorable in biomedical applications.

3.2.2. Influence of SF incorporation on the swelling ratio of HAP

The swelling ability of the material was the key factor for transmitting nutrients and minerals to enhance bone cell growth. Moreover, the degree of swelling plays the most important role in artificial scaffolds [55]. Fig. 6 shows the swelling ability of the nanocomposite scaffolds in SBF medium.

From the figure, it is evident that the absorption ability of the nanocomposites was higher in comparison with pristine HAP. Also, it was confirmed that the swelling ratio of SF increased with the SF concentration. This result was in good agreement with the degradation results. The swelling ratio of the nanocomposites scaffolds is reduced after 15 days that may due to the formation of minerals on the surface of the scaffold. An increase in the swelling ratio of the nanocomposite scaffolds are mainly due to the higher hydrophilic surface nature of SF in the HS-3 [56]. Silk fibroin contains both hydrophilic (random coil), and hydrophobic (β-sheet) blocks of amino acids, which were confirmed by the FTIR results. Hydrophobic block was responsible for the stability of the scaffold, while the hydrophilic block was responsible for the cell adhesion, proliferation and swelling ability of the scaffold. The presence of nano-sized pores particle in the nanocomposite's scaffolds enhance the swelling ratio through cell infusion into the scaffolds as well as cell adhesion [57].

3.2.3. Influence of SF incorporation on the biomineralization of hydroxyapatite

Bioactivity of the scaffolds was tested using the *in-vitro* biomineralization study. Different HAP/SF ratio nanocomposite pellet was immersed in SBF for 15 days to confirm the biomineralization ability of the nanocomposite scaffolds. A remarkable difference in the weight of the pellet has been observed with the prolongation of the incubation time. The deposition of the apatite shows the obvious weight increase of the scaffold. Meanwhile, it was also seen that the weight of the scaffolds improved with an increase in the SF concentration for the same incubation period. It might be due to the presence of densely occupied hydroxyl groups in the nanocomposite scaffolds [58]. Those hydroxyl groups ionize in the SBF to form a negatively charged surface to initiate the initial nucleation site which attracts the calcium ions. Further, the pellets were collected and dried, then studied using FTIR and XRD analysis.

FTIR spectra of pristine HAP and composites were depicted in

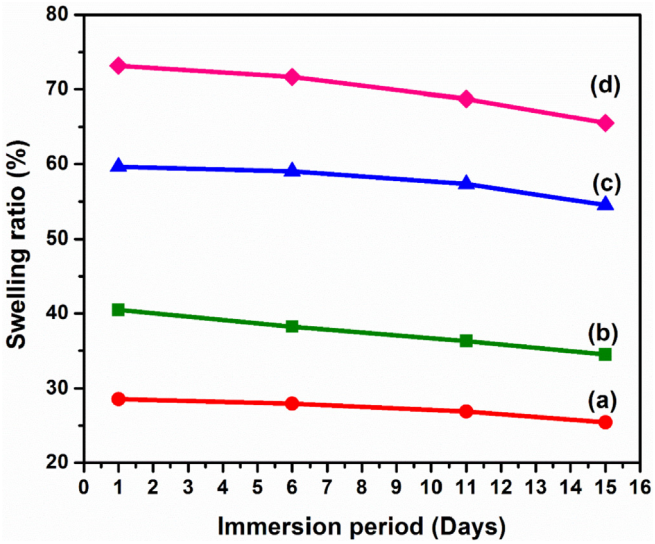

Fig. 6. Swelling ratio of (a) Pristine HAP (b) HS-1 (c) HS-2 and (d) HS-3 nanocomposites post immersion in SBF solution.

Fig. 7. The FTIR spectra clearly shows all the scaffolds precipitate, apatite minerals from the SBF solution which was evident from the increased intensity of phosphate and OH groups in all scaffolds. XRD characterization technique was used to confirm the crystalline structure of the mineral formed in the SBF solution after 15 days of immersion period and the results are shown in Fig. 8. During the immersion period, the peak intensity of all the scaffolds was increased. There was no evidence of peaks other than HAP. Peak broadening was attributed to the amorphous nature of apatite.

The *in-vitro* study shows that among all scaffolds, the HS-3 scaffold showed considerable degradation along with the high rate of mineralization. SBF was a meta-stable solution that had ion concentrations equal to human blood plasma, supersaturated with respect to apatite. In SBF solution mineralization was induced by an external stimulus because the barrier for homogeneous nucleation of apatite was high since both HAP and SF acts as a nucleation site for mineral deposition. It reveals that the biological activity of artificial scaffolds is closely related to their structural characteristics. Biodegradability and biomineralization of the scaffolds are highly depended on the content of the secondary structure of silk fibroin. The results of the current study consistently showed that the presence of SF is effective in supporting the proliferation of new cells through the production of specific proteins which results in a large amount of mineralized tissue formation.

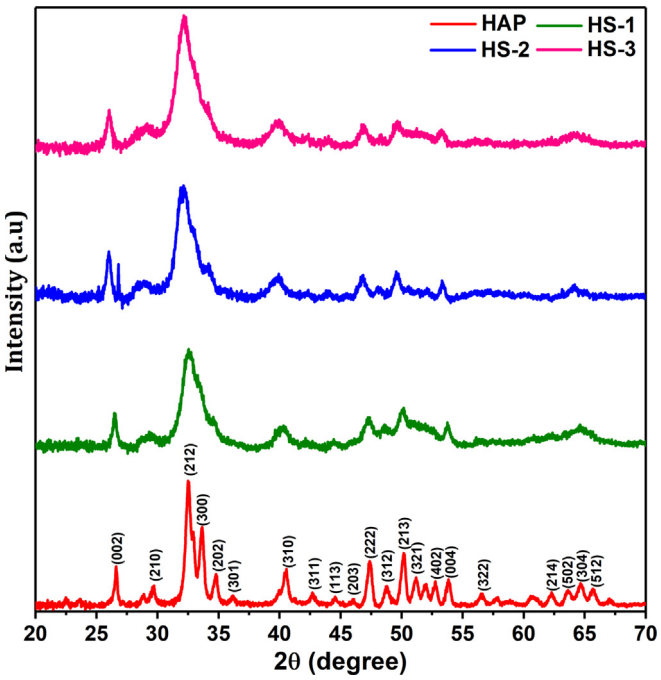

Fig. 8. XRD pattern of each fabricated samples in SBF solutions on day 15.

4. Conclusion

A potentially bioactive HAP/SF nanocomposite were prepared by the *in-situ* co-precipitation method to determine its bioactivity for bone tissue engineering. The FTIR spectra of the HAP/SF composites confirmed the presence of PO_4^{3-} in all the composites with silk-I and silk-II groups. The formation of β-sheet structure from random coil was confirmed from shift in the band position of amide-I from 1651 cm^{-1} to 1621, 1624 and 1627 cm^{-1} in HS-1, HS-2 and HS-3 composites respectively. The decrease in the crystallite size of HS-3 nanocomposite (14 nm) in comparison with pristine HAP (30 nm) reflects the obstructive role of SF, resulting in constrained growth of HAP and successful formation of HS nanocomposite. The surface morphology of HAP from needle-like rod to spongy spherical shaped particles confirms the presence of SF and HAP in the HS nanocomposite with decreased size. *In-vitro* bioactivity of the HS composite reveals the hike in the biodegradation, swelling and biomineralization ability with an increase in SF content that favors cell adhesion. The degradation rate of HS-3 composite decreased from 11% to 8% in the SBF solution which can be associated with the biomineralization due to an increase in SF content. The SF to HAP ratio in HS-3 composite was found to be higher than the others which substantially improved the biodegradation and biomineralization of the scaffold. Thus, the incorporation of SF into HAP proves to be a more efficient way in the production of better scaffolds for bone tissue engineering.

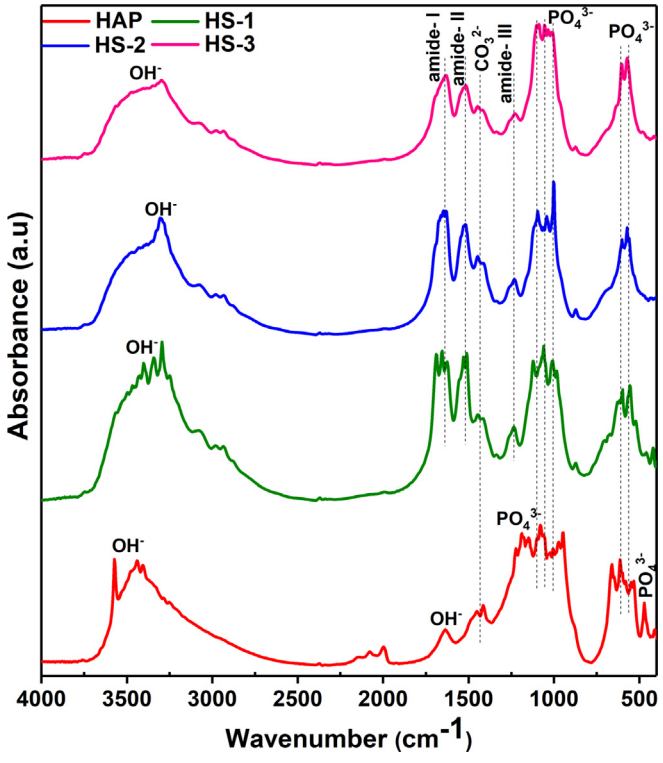

Fig. 7. FTIR spectra of prepared samples after 15 days of incubation in SBF solution.

CRediT authorship contribution statement

J. Mobika: Conceptualization, Writing - original draft. **M. Rajkumar:** Supervision. **V. Nithya Priya:** Formal analysis. **S.P. Linto Sibi:** Writing - review & editing.

References

[1] A.K. Teotia, D.B. Raina, C. Singh, N. Sinha, H. Isaksson, M. Tägil, L. Lidgren, A. Kumar, Nano-hydroxyapatite bone substitute functionalized with bone active molecules for enhanced cranial bone regeneration, ACS Appl. Mater. Interfaces 9 (2017) 6816–6828, https://doi.org/10.1021/acsami.6b14782.

[2] S. Behera, D. Naskar, S. Sapru, P. Bhattacharjee, T. Dey, A.K. Ghosh, M. Mandal, S.C. Kundu, Hydroxyapatite reinforced inherent RGD containing silk fibroin composite scaffolds: promising platform for bone tissue engineering, Nanomed. Nanotechnol. Biol. Med. 13 (2017) 1745–1759, https://doi.org/10.1016/j.nano.2017.02.016.

[3] R. Murugan, S. Ramakrishna, Bioresorbable composite bone paste using polysaccharide based nano hydroxyapatite, Biomaterials 25 (2004) 3829–3835, https://doi.org/10.1016/j.biomaterials.2003.10.016.

[4] K.M. Sajesh, K. Kiran, S.V. Nair, R. Jayakumar, Sequential layer-by-layer electrospinning of nano SrCO3/PRP loaded PHBV fibrous scaffold for bone tissue engineering, Compos. B Eng. 99 (2016) 445–452, https://doi.org/10.1016/

j.compositesb.2016.06.026.
[5] K. Pietrucha, Physicochemical properties of 3D collagen-CS scaffolds for potential use in neural tissue engineering, Int. J. Biol. Macromol. 80 (2015) 732–739, https://doi.org/10.1016/j.ijbiomac.2015.07.005.
[6] E.J. Shin, S.M. Choi, D. Singh, S.M. Zo, Y.H. Lee, J.H. Kim, S.S. Han, Fabrication of cellulose-based scaffold with microarchitecture using a leaching technique for biomedical applications, Cellulose 21 (2014) 3515–3525, https://doi.org/10.1007/s10570-014-0368-2.
[7] C. Ao, Y. Niu, X. Zhang, X. He, W. Zhang, C. Lu, Fabrication and characterization of electrospun cellulose/nano-hydroxyapatite nanofibers for bone tissue engineering, Int. J. Biol. Macromol. 97 (2017) 568–573, https://doi.org/10.1016/j.ijbiomac.2016.12.091.
[8] C. Tsai, C. Hung, C. Kuo, C. Chen, Y.-N. Peng, M.-Y. Shie, Improved bioactivity of 3D printed porous titanium alloy scaffold with chitosan/magnesium-calcium silicate composite for orthopaedic applications, Materials 12 (2019) 203, https://doi.org/10.3390/ma12020203.
[9] D.K. Kim, J.I. Kim, T.I. Hwang, B.R. Sim, G. Khang, Bioengineered osteoinductive broussonetia kazinoki/silk fibroin composite scaffolds for bone tissue regeneration, ACS Appl. Mater. Interfaces 9 (2017) 1384–1394, https://doi.org/10.1021/acsami.6b14351.
[10] A. Ficai, E. Andronescu, G. Voicu, C. Ghitulica, D. Ficai, The influence of collagen support and ionic species on the morphology of collagen/hydroxyapatite composite materials, Mater. Char. 61 (2010) 402–407, https://doi.org/10.1016/j.matchar.2010.01.003.
[11] M. Iafisco, N. Margiotta, Silica xerogels and hydroxyapatite nanocrystals for the local delivery of platinum-bisphosphonate complexes in the treatment of bone tumors: a mini-review, J. Inorg. Biochem. 117 (2012) 237–247, https://doi.org/10.1016/j.jinorgbio.2012.06.004.
[12] Z. Cui, W. Li, L. Cheng, D. Gong, W. Cheng, W. Wang, Effect of nano-HA content on the mechanical properties, degradation and biocompatible behavior of Mg-Zn/HA composite prepared by spark plasma sintering, Mater. Char. 151 (2019) 620–631, https://doi.org/10.1016/j.matchar.2019.03.048.
[13] D. Sivaraj, K. Vijayalakshmi, Novel synthesis of bioactive hydroxyapatite/f-multiwalled carbon nanotube composite coating on 316L SS implant for substantial corrosion resistance and antibacterial activity, J. Alloy. Comp. 777 (2019) 1340–1346, https://doi.org/10.1016/j.jallcom.2018.10.341.
[14] G. Goller, H. Demirkiran, F.N. Oktar, E. Demirkesen, Processing and characterization of bioglass reinforced hydroxyapatite composites, Ceram. Int. 29 (2003) 721–724, https://doi.org/10.1016/S0272-8842(02)00223-7.
[15] R.D. Welch, B. Hudson Berry, K. Crawford, H. Zhang, M. Zobitz, D. Bronson, S. Krishnan, Subchondral defects in caprine femora augmented with in situ setting hydroxyapatite cement, polymethylmethacrylate, or autogenous bone graft: biomechanical and histomorphological analysis after two-years, J. Orthop. Res. 20 (2002) 464–472, https://doi.org/10.1016/S0736-0266(01)00124-3.
[16] M. Jeon, S. Jung, S. Park, Facile covalent bio-conjugation of hydroxyapatite, New J. Chem. 42 (2018) 14870–14875, https://doi.org/10.1039/c8nj02766h.
[17] M. Sarker, X.B. Chen, D.J. Schreyer, Experimental approaches to vascularisation within tissue engineering constructs, J. Biomater. Sci. Polym. Ed. 26 (2015) 683–734, https://doi.org/10.1080/09205063.2015.1059018.
[18] K. Szurkowska, A. Zgadzaj, M. Kuras, J. Kolmas, Novel hybrid material based on Mg 2+ and SiO 44- co-substituted nano-hydroxyapatite, alginate and chondroitin sulphate for potential use in biomaterials engineering, Ceram. Int. 44 (2018) 18551–18559, https://doi.org/10.1016/j.ceramint.2018.07.077.
[19] C. Cao, H. Li, J. Li, C. Liu, H. Yang, B. Li, Mechanical reinforcement of injectable calcium phosphate cement/silk fibroin (SF) composite by mineralized SF, Ceram. Int. 40 (2014) 13987–13993, https://doi.org/10.1016/j.ceramint.2014.05.123.
[20] S. Shanmugavel, V.J. Reddy, S. Ramakrishna, B.S. Lakshmi, V.G. Dev, Precipitation of hydroxyapatite on electrospun polycaprolactone/aloe vera/silk fibroin nanofibrous scaffolds for bone tissue engineering, J. Biomater. Appl. 29 (2014) 46–58, https://doi.org/10.1177/0885328213513934.
[21] Perteghella, Coccè Sottani, Cavicchini Negri, Cottica Alessandri, Grignani Torre, Pessina, paclitaxel-loaded silk fibroin nanoparticles: method validation by UHPLC-MS/MS to assess an exogenous approach to load cytotoxic drugs, Pharmaceutics 11 (2019) 285, https://doi.org/10.3390/pharmaceutics11060285.
[22] J. Ran, J. Hu, G. Sun, S. Chen, L. Chen, X. Shen, H. Tong, Comparisons between gelatin-tussah silk fibroin/hydroxyapatite and gelatin-Bombyx mori silk fibroin/hydroxyapatite nano-composites for bone tissue engineering, RSC Adv. 5 (2015) 76526–76537, https://doi.org/10.1039/c5ra14279b.
[23] R. Bhowmik, K.S. Katti, D. Katti, Molecular dynamics simulation of hydroxyapatite-polyacrylic acid interfaces, Polymer 48 (2007) 664–674, https://doi.org/10.1016/j.polymer.2006.11.015.
[24] T.Y. Liu, S.Y. Chen, D.M. Liu, S.C. Liou, On the study of BSA-loaded calcium-deficient hydroxyapatite nano-carriers for controlled drug delivery, J. Control. Release 107 (2005) 112–121, https://doi.org/10.1016/j.jconrel.2005.05.025.
[25] S. Moeini, M.R. Mohammadi, A. Simchi, In-situ solvothermal processing of polycaprolactone/hydroxyapatite nanocomposites with enhanced mechanical and biological performance for bone tissue engineering, Bioact. Mater. 2 (2017) 146–155, https://doi.org/10.1016/j.bioactmat.2017.04.004.
[26] Y. Tang, Y. Du, Y. Li, X. Wang, X. Hu, A thermosensitive chitosan/poly(vinyl alcohol) hydrogel containing hydroxyapatite for protein delivery, J. Biomed. Mater. Res. A 91 (2009) 953–963, https://doi.org/10.1002/jbm.a.32240.
[27] M. Li, M.J. Mondrinos, X. Chen, M.R. Gandhi, F.K. Ko, P.I. Lelkes, Elastin blends for tissue engineering scaffolds, J. Biomed. Mater. Res. A 79 (2006) 963–973, https://doi.org/10.1002/jbm.a.
[28] H.J. Kim, M.K. Kim, K.H. Lee, S.K. Nho, M.S. Han, I.C. Um, Effect of degumming methods on structural characteristics and properties of regenerated silk, Int. J. Biol. Macromol. 104 (2017) 294–302, https://doi.org/10.1016/j.ijbiomac.2017.06.019.
[29] Z. Liu, F. Zhang, J. Ming, S. Bie, J. Li, B. Zuo, Preparation of electrospun silk fibroin nanofibers from solutions containing native silk fibrils, J. Appl. Polym. Sci. 132 (2015) 1–7, https://doi.org/10.1002/app.41236.
[30] H. Chakraborty, N. Bhowmik, Structure and stability analysis of biocompatible hydroxyapatite reinforced chitosan nanocomposite, Polym. Compos. 39 (2018) E573–E583, https://doi.org/10.1002/pc.24726.
[31] T. Kokubo, H. Takadama, How useful is SBF in predicting in vivo bone bioactivity? Biomaterials 27 (2006) 2907–2915, https://doi.org/10.1016/j.biomaterials.2006.01.017.
[32] Z. Hadisi, J. Nourmohammadi, J. Mohammadi, Composite of porous starch-silk fibroin nanofiber-calcium phosphate for bone regeneration, Ceram. Int. 41 (2015) 10745–10754, https://doi.org/10.1016/j.ceramint.2015.05.010.
[33] B. Mondal, S. Mondal, A. Mondal, N. Mandal, Fish scale derived hydroxyapatite scaffold for bone tissue engineering, Mater. Char. 121 (2016) 112–124, https://doi.org/10.1016/j.matchar.2016.09.034.
[34] A.A. Lozano-Pérez, A.L. Gil, S.A. Pérez, N. Cutillas, H. Meyer, M. Pedreño, S.D. Aznar-Cervantes, C. Janiak, J.L. Cenis, J. Ruiz, Antitumor properties of platinum(IV) prodrug-loaded silk fibroin nanoparticles, Dalton Trans. 44 (2015) 13513–13521, https://doi.org/10.1039/c5dt00378d.
[35] A. Teimouri, M. Azadi, R. Emadi, J. Lari, A.N. Chermahini, Preparation, characterization, degradation and biocompatibility of different silk fibroin based composite scaffolds prepared by freeze-drying method for tissue engineering application, Polym. Degrad. Stab. 121 (2015) 18–29, https://doi.org/10.1016/j.polymdegradstab.2015.08.004.
[36] L. Lin, R. Hao, W. Xiong, J. Zhong, Quantitative analyses of the effect of silk fibroin/nano-hydroxyapatite composites on osteogenic differentiation of MG-63 human osteosarcoma cells, J. Biosci. Bioeng. 119 (2015) 591–595, https://doi.org/10.1016/j.jbiosc.2014.10.009.
[37] Y. Wang, J. Dai, Q. Zhang, Y. Xiao, M. Lang, Improved mechanical properties of hydroxyapatite/poly(ε-caprolactone) scaffolds by surface modification of hydroxyapatite, Appl. Surf. Sci. 256 (2010) 6107–6112, https://doi.org/10.1016/j.apsusc.2010.03.127.
[38] E.I. Paşcu, J. Stokes, G.B. McGuinness, Electrospun composites of PHBV, silk fibroin and nano-hydroxyapatite for bone tissue engineering, Mater. Sci. Eng. C 33 (2013) 4905–4916, https://doi.org/10.1016/j.msec.2013.08.012.
[39] F. Mohandes, M. Salavati-Niasari, Influence of morphology on the in vitro bioactivity of hydroxyapatite nanostructures prepared by precipitation method, New J. Chem. 38 (2014) 4501–4509, https://doi.org/10.1039/c4nj00649f.
[40] S. Agrawal, M. Kelkar, A. De, A.R. Kulkarni, M.N. Gandhi, Surfactant free novel one-minute microwave synthesis, characterization and cell toxicity study of mesoporous strontium hydroxyapatite nanorods, RSC Adv. 6 (2016) 94921–94926, https://doi.org/10.1039/c6ra21708g.
[41] G. Karunakaran, G.S. Kumar, E.B. Cho, Y. Sunwoo, E. Kolesnikov, D. Kuznetsov, Microwave-assisted hydrothermal synthesis of mesoporous carbonated hydroxyapatite with tunable nanoscale characteristics for biomedical applications, Ceram. Int. 45 (2019) 970–977, https://doi.org/10.1016/j.ceramint.2018.09.273.
[42] K. Wei, Y. Li, K.-O. Kim, Y. Nakagawa, B.-S. Kim, K. Abe, G.-Q. Chen, I.-S. Kim, Fabrication of nano-hydroxyapatite on electrospun silk fibroin nanofiber and their effects in osteoblastic behavior, J. Biomed. Mater. Res. A 97A (2011) 272–280, https://doi.org/10.1002/jbm.a.33054.
[43] N. Hassani Besheli, F. Mottaghitalab, M. Eslami, M. Gholami, S.C. Kundu, D.L. Kaplan, M. Farokhi, Sustainable release of vancomycin from silk fibroin nanoparticles for treating severe bone infection in rat tibia osteomyelitis model, ACS Appl. Mater. Interfaces 9 (2017) 5128–5138, https://doi.org/10.1021/acsami.6b14912.
[44] S. Lu, J. Li, S. Zhang, Z. Yin, T. Xing, D.L. Kaplan, The influence of the hydrophilic-lipophilic environment on the structure of silk fibroin protein, J. Mater. Chem. B. 3 (2015) 2599–2606, https://doi.org/10.1039/c4tb01873g.
[45] S. Teng, L. Chen, Y. Guo, J. Shi, Formation of nano-hydroxyapatite in gelatin droplets and the resulting porous composite microspheres, J. Inorg. Biochem. 101 (2007) 686–691, https://doi.org/10.1016/j.jinorgbio.2006.11.018.
[46] H. El Khal, N. Harrouch Batis, Effects of temperature on the preparation and characteristics of hydroxyapatite and its adsorptive properties toward lead, New J. Chem. 39 (2015) 3597–3607, https://doi.org/10.1039/c4nj01836b.
[47] S. Elangomannan, K. Louis, B.M. Dharmaraj, V.S. Kandasamy, K. Soundarapandian, D. Gopi, Carbon nanofiber/polycaprolactone/mineralized hydroxyapatite nanofibrous scaffolds for potential orthopedic applications, ACS Appl. Mater. Interfaces 9 (2017) 6342–6355, https://doi.org/10.1021/acsami.6b13058.
[48] D. Van Hong Thien, S.W. Hsiao, M.H. Ho, C.H. Li, J.L. Shih, Electrospun chitosan/hydroxyapatite nanofibers for bone tissue engineering, J. Mater. Sci. 48 (2013) 1640–1645, https://doi.org/10.1007/s10853-012-6921-1.
[49] W. Zhang, J.X. He, S.Z. Cui, Preparation and research of tussah silk fibroin/hydroxyapatite composites, Adv. Mater. Res. 152–153 (2010) 734–738, https://doi.org/10.4028/www.scientific.net/AMR.152-153.734.
[50] G.-X. Cao, D.-Y. Xu, M.-Z. Zhou, Z.-F. Liao, Y.-D. Wang, A novel high strength porous hydroxyapatite/silk fibroin composite: preparation and

characterization, in: Proc. 2nd Annu. Int. Conf. Adv. Mater. Eng. (AME 2016), Atlantis Press, Paris, France, 2016, pp. 142–145, https://doi.org/10.2991/ame-16.2016.24.
[51] H. Cao, X. Chen, J. Yao, Z. Shao, Fabrication of an alternative regenerated silk fibroin nanofiber and carbonated hydroxyapatite multilayered composite via layer-by-layer, J. Mater. Sci. 48 (2013) 150–155, https://doi.org/10.1007/s10853-012-6722-6.
[52] S.C.G. Leeuwenburgh, J. Jo, H. Wang, M. Yamamoto, J.A. Jansen, Y. Tabata, Mineralization, biodegradation, and drug release behavior of gelatin/apatite composite microspheres for bone regeneration, Biomacromolecules 11 (2010) 2653–2659, https://doi.org/10.1021/bm1006344.
[53] Y. Hu, X. Gu, Y. Yang, J. Huang, M. Hu, W. Chen, Z. Tong, C. Wang, Facile fabrication of poly (L-lactic acid) -grafted hydroxyapatite/poly (lactic-co-glycolic acid) scaffolds by pickering high internal phase emulsion templates, ACS Appl. Mater. Interfaces 6 (2014) 17166–17175, https://doi.org/10.1021/am504877h.
[54] C. Vepari, D.L. Kaplan, Silk as a biomaterial, Prog. Polym. Sci. 32 (2007) 991–1007, https://doi.org/10.1016/j.progpolymsci.2007.05.013.
[55] M. Peter, N. Ganesh, N. Selvamurugan, S.V. Nair, T. Furuike, H. Tamura, R. Jayakumar, Preparation and characterization of chitosan-gelatin/nanohydroxyapatite composite scaffolds for tissue engineering applications, Carbohydr. Polym. 80 (2010) 687–694, https://doi.org/10.1016/j.carbpol.2009.11.050.
[56] C. Sharma, A.K. Dinda, P.D. Potdar, C.F. Chou, N.C. Mishra, Fabrication and characterization of novel nano-biocomposite scaffold of chitosan-gelatin-alginate-hydroxyapatite for bone tissue engineering, Mater. Sci. Eng. C 64 (2016) 416–427, https://doi.org/10.1016/j.msec.2016.03.060.
[57] H. Kweon, H.C. Ha, I.C. Um, Y.H. Park, Physical properties of silk fibroin/chitosan blend films, J. Appl. Polym. Sci. 80 (2001) 928–934, https://doi.org/10.1002/app.1172.
[58] Y.Z. Wan, Y. Huang, C.D. Yuan, S. Raman, Y. Zhu, H.J. Jiang, F. He, C. Gao, Biomimetic synthesis of hydroxyapatite/bacterial cellulose nanocomposites for biomedical applications, Mater. Sci. Eng. C 27 (2007) 855–864, https://doi.org/10.1016/j.msec.2006.10.002.